Supporting Information

Size-optimized Ultrasmall Porous Silica Nanoparticles Depict Vasculature-based Differential Targeting in Triple Negative Breast Cancer

Shreya Goel, Carolina A. Ferreira[‡], Prashant Dogra[‡], Bo Yu, Christopher J. Kutyreff, Cerise M. Siamof, Jonathan W. Engle, Todd E. Barnhart, Vittorio Cristini, Zhihui Wang*, Weibo Cai*

S1. Supplementary materials and methods

Materials

Tetramethyl orthosilicate (TMOS), hexadecyltrimethylammonium bromide (CTAB), 2.0 M ammonium hydroxide solution were purchased from Sigma-Aldrich (St. Louis, MO). PD-10 columns were purchased from GE Healthcare (Piscataway, NJ). Absolute ethanol, acetic acid and doxorubicin hydrochloride (DOX) were purchased from Fisher Scientific. Water and all buffers were of Millipore grade and pretreated with Chelex 100 resin to ensure that the aqueous solution was free of heavy metals. All chemicals were used as received without further purification. PEG-silane and NH_2-PPO-silane were purchased from Gelest.

Cell culture and tumor models

Triple negative murine 4T1 and human MDA-MB 231 tumor cell lines were purchased from American Type Culture Collection (ATCC, Manassas, VA) and cultured in Roswell Park Memorial Institute (RPMI 1640) and Dulbecco's Modified Eagle Medium (DMEM), respectively, supplemented with 10 % fetal bovine serum (FBS) and 1 % pencillin-streptomycin at 37 °C with 5 % CO_2.

All animal studies were carried out according to the University of Wisconsin Institutional Animal Care and Use Committee (IACUC) guidelines. Female Balb/c mice (4-6 weeks old) and female athymic nude mice (6-8 weeks old) were purchased from Envigo (Indianapolis, IN). Subcutaneous 4T1 tumors were generated by implanting 1×10^6 cells suspended in 100 µL PBS

in the front or hind flanks of Balb/c mice. To generate MDA-MB 231 tumors, athymic nude mice were implanted with 2×10^6 cells suspended in 50 µL of 1:1 mixture of PBS: Matrigel (Corning, NY). Tumor growth was monitored every other day and mice were used for in vivo studies when the tumors reached 5- 8 mm in diameter.

Mathematical model structure

To understand and describe the whole-body tissue disposition kinetics of UPSNs, we developed a simplified physiologically based pharmacokinetic (PBPK) model in healthy and tumor-bearing animals, based on previously developed models (see schematic in Fig. 2C).[1] The model consists of four obligatory (plasma, liver, spleen, and muscle) and one facultative (tumor) compartment, which represent the dominant distribution sites of the UPSNs *in vivo*, connected in an anatomical fashion via plasma (red arrows) and lymph (blue arrows) flow. The plasma compartment is the central compartment, and supplies arterial blood to and receives venous blood from all the compartments, except the spleen, which feeds its venous return into the liver (via portal vein), thereby implementing dual blood supply to the liver (via hepatic artery and portal vein). Every compartment, except plasma, is further partitioned into vascular (red) and extravascular (blue) sub-compartments. Additionally, the liver and spleen have a phagocytic sub-compartment (green) to investigate the sequestration of systemically injected NPs by phagocytes. A phagocytic sub-compartment is not incorporated in the muscle compartment, given that the muscles are not a part of the RES and thus do not have a significant presence of resident macrophages. No further compartmentalization is implemented for the tumor compartment. Instead of plasma and lymph flow rates, it communicates with the plasma compartment via phenomenological first order inflow (k_{in}) and outflow (k_{out}) rate constants. Note that renal excretion is negligible for NPs > 10 nm, therefore a kidney compartment was not included in the model [2], thus hepatobiliary excretion formed the basis of UPSN clearance.

S2. Model Equations

The model consists of the following system of equations:

2

Plasma

$$\frac{dN_P}{dt} = \frac{N_{e,S}}{V_{e,S}} L_S + \frac{N_{e,L}}{V_{e,L}} L_L + \frac{N_{e,M}}{V_{e,M}} L_M + \frac{N_{v,L}}{V_{v,L}} \left(\tilde{Q}_L - L_L \right) + \frac{N_{v,M}}{V_{v,M}} (Q_M - L_M) + N_T k_{out} - \frac{N_P}{V_P} (Q_S +$$

$$Q_L + Q_G + Q_M) - N_P k_{in},$$

$$N_P(0) = N_0 \quad \text{(S1)}$$

where N_P is the mass of NPs in systemic blood; $N_{e,i}$ and $N_{v,i}$ represent the mass of NPs in the extravascular and vascular sub-compartments of organ i (i $= S, L, M,$ and T for spleen, liver, muscle, and tumor, respectively), and N_T is the mass of NPs in tumor compartment; $V_{e,i}$ and $V_{v,i}$ represent the volume of the extravascular and vascular sub-compartments of organ i, respectively, and V_P represents the volume of systemic blood; Q_i and L_i represent plasma and lymph flow rates pertinent to organ i (i $= G$ for gut, not modeled explicitly though), respectively; note, $\tilde{Q}_L = Q_L + Q_G + Q_S - L_S$, is the plasma flow rate into the liver from hepatic artery (Q_L) and portal vein ($Q_G + Q_S - L_S$) combined; σ_i ($0 \leq \sigma_i \leq 1$) is the vascular reflection coefficient of organ i; and k_{in} and k_{out} represent the phenomenological first order inflow and outflow rate constants of the tumor compartment, respectively. N_0 is the injected mass of NPs (i.e. 100 % ID).

Spleen

$$\frac{dN_{v,S}}{dt} = \frac{N_P}{V_P} Q_S - \frac{N_{v,S}}{V_{v,S}} (Q_S - L_S) - \frac{N_{v,S}}{V_{v,S}} L_S \cdot (1 - \sigma_S) - N_{v,S} \cdot k_{phag}, \qquad N_{v,S}(0) =$$

$$0 \quad \text{(S2)}$$

$$\frac{dN_{e,S}}{dt} = \frac{N_{v,S}}{V_{v,S}} L_S \cdot (1 - \sigma_S) - \frac{N_{e,S}}{V_{e,S}} L_S - \frac{N_{e,S}}{V_{e,S}} B, \qquad N_{e,S}(0) =$$

$$0 \quad \text{(S3)}$$

$$\frac{dN_{p,S}}{dt} = N_{v,S} \cdot k_{phag} - N_{p,S} \cdot k_{ex}, \qquad N_{p,S}(0) =$$

$$0 \quad \text{(S4)}$$

where $N_{p,i}$ represents the mass of NPs in the phagocytic sub-compartment of organ i; k_{phag} and $k_{ex,i}$ describe the phagocytic uptake rate and the excretion rate from phagocytes, respectively; B is the bile flow rate.

Liver

$$\frac{dN_{v,L}}{dt} = \frac{N_P}{V_P}(Q_L + Q_G) + \frac{N_{v,S}}{V_{v,S}}(Q_S - L_S) - \frac{N_{v,L}}{V_{v,L}}(\tilde{Q}_L - L_L) - \frac{N_{v,L}}{V_{v,L}}L_L \cdot (1 - \sigma_L) - N_{v,L} \cdot k_{phag},$$

$$N_{v,L}(0) = 0$$

(S5)

$$\frac{dN_{e,L}}{dt} = \frac{N_{v,L}}{V_{v,L}}L_L \cdot (1 - \sigma_L) - \frac{N_{e,L}}{V_{e,L}}L_L - \frac{N_{e,L}}{V_{e,L}}B, \qquad N_{e,L}(0) =$$

0   (S6)

$$\frac{dN_{p,L}}{dt} = N_{v,L} \cdot k_{phag} - N_{p,L} \cdot k_{ex}, \qquad N_{p,L}(0) =$$

0   (S7)

Muscle

$$\frac{dN_{v,M}}{dt} = \frac{N_P}{V_P}Q_M - \frac{N_{v,M}}{V_{v,M}}(Q_M - L_M) - \frac{N_{v,M}}{V_{v,M}}L_M \cdot (1 - \sigma_M), \qquad N_{v,M}(0) =$$

0   (S8)

$$\frac{dN_{e,M}}{dt} = \frac{N_{v,M}}{V_{v,M}}L_M \cdot (1 - \sigma_M) - \frac{N_{e,M}}{V_{e,M}}L_M, \qquad N_{e,M}(0) =$$

0   (S9)

Tumor

$$\frac{dN_T}{dt} = N_P k_{in} - N_T k_{out}, \qquad N_T(0) = 0$$

(S10)

Excretion

$$\frac{dN_{ex}}{dt} = (N_{p,S} + N_{p,L}) \cdot k_{ex} + \left(\frac{N_{e,S}}{V_{e,S}} + \frac{N_{e,L}}{V_{e,L}}\right)B, \qquad N_{ex}(0) = 0$$
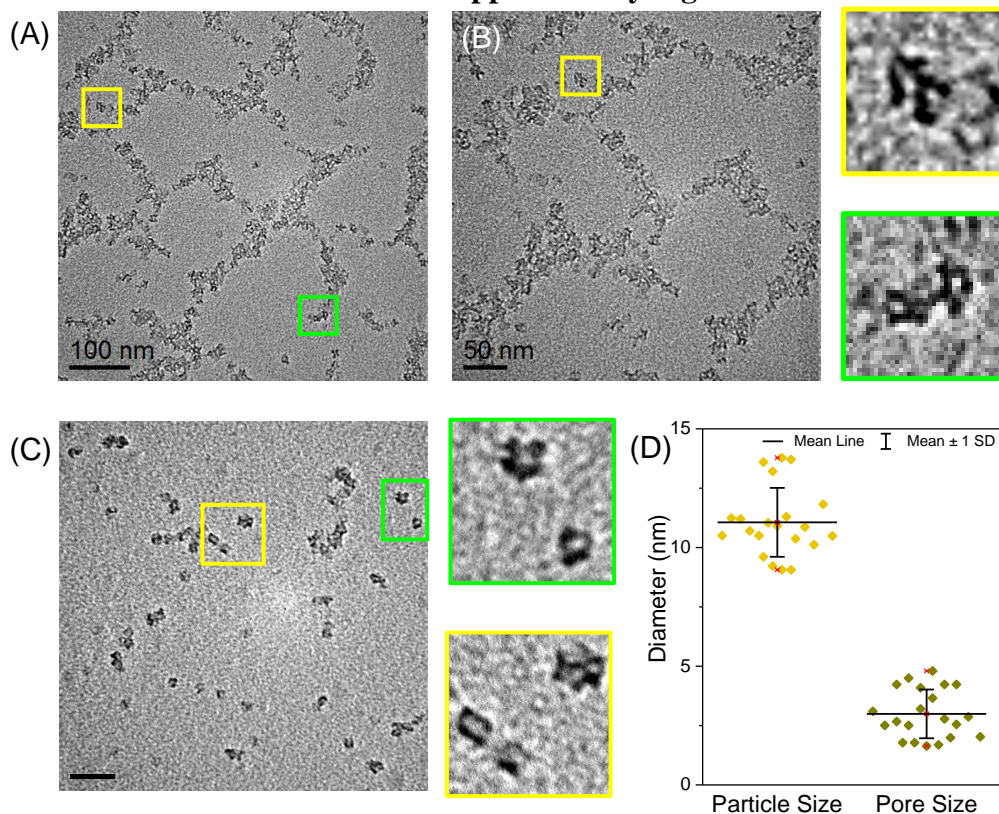
(S11)

4

Supplementary Figures

Figure S1. Transmission electron microscopy (TEM) of UPSN at (A) lower and (B) higher magnification. Outsets in yellow and green boxes depict higher zoomed-in image of UPSNs with half-pore and single full pore morphologies, respectively. (C) TEM image of UPSN-NOTA, with outsets showing preservation of pore structure post surface modification. Yellow box shows half-pore and green box shows full-pore microstructural details. (D) Average particle and pore diameters of UPSN, determined from TEM images. Each data point depicts average of atleast 10 particles per field of view. Atleast 20 fields were analyzed for measurement. Black lines represent mean ± SD.
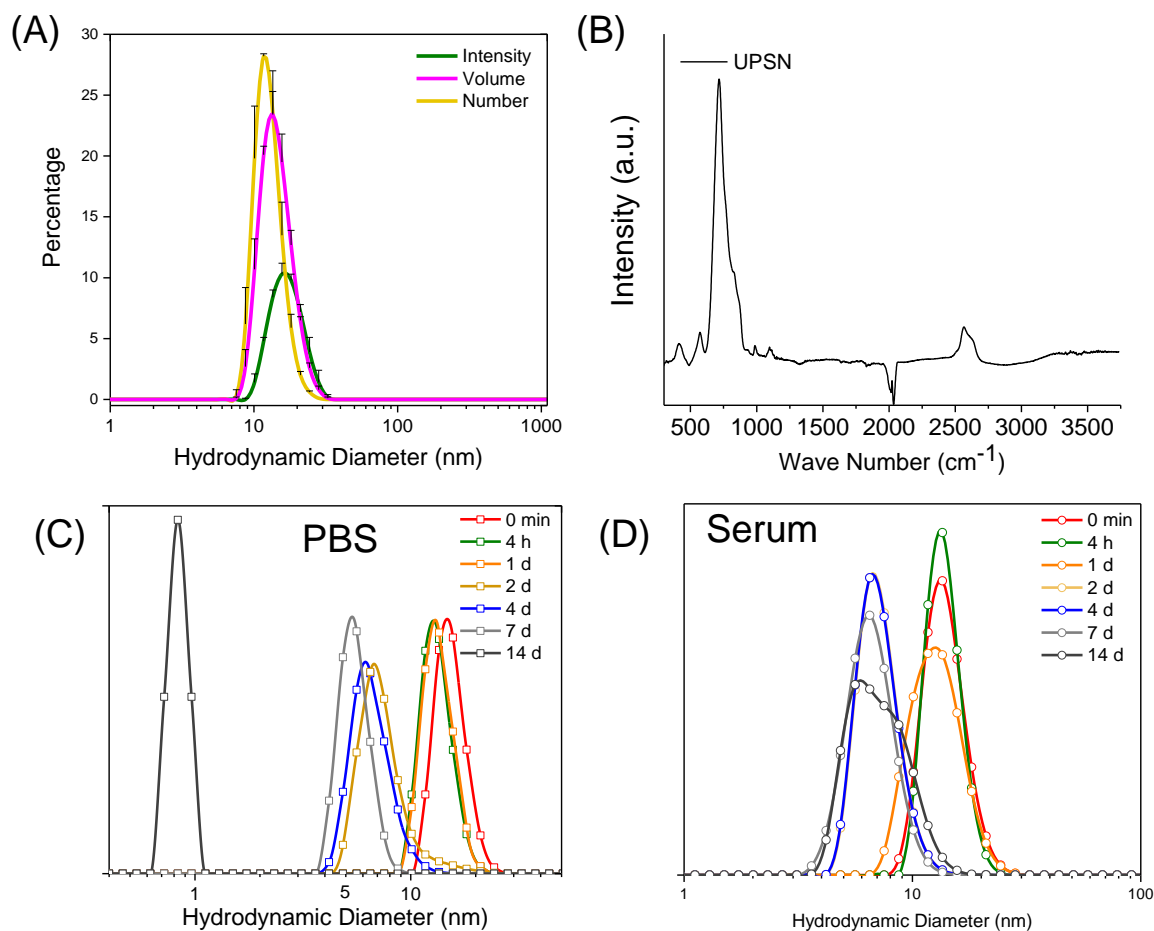
Figure S2. (A) DLS measurements of hydrodynamic diameter of UPSN by intensity, volume, and number, after 6 months of storage in water at 4 °C. (B) Transmission FTIR of aqueous UPSN solution indicating the formation of silica core, presence of PEG chain, and absence of CTAB surfactant in the final construct. (C-D) DLS measurements indicating time-dependent disintegration of UPSN in PBS and serum, tested over 2 weeks.
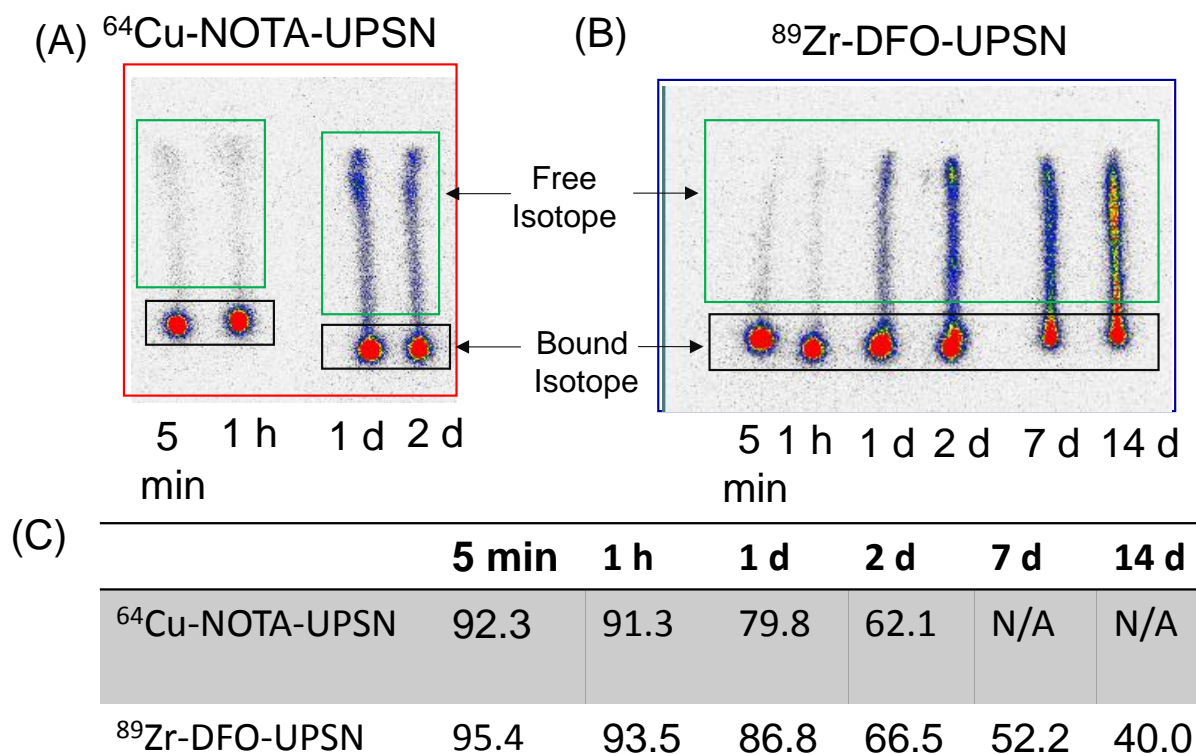
(A) ^{64}Cu-NOTA-UPSN   (B) ^{89}Zr-DFO-UPSN

Free Isotope

Bound Isotope

5 min   1 h   1 d   2 d

5 min   1 h   1 d   2 d   7 d   14 d

(C)

	5 min	1 h	1 d	2 d	7 d	14 d
^{64}Cu-NOTA-UPSN	92.3	91.3	79.8	62.1	N/A	N/A
^{89}Zr-DFO-UPSN	95.4	93.5	86.8	66.5	52.2	40.0

Figure S3. (A-B) Thin layer chromatograms (TLC) from *in vitro* serum stability test of ^{64}Cu-NOTA-UPSN and ^{89}Zr-DFO-UPSN over 2 and 14 days, respectively, indicating the radioactivity retained at the origin (bound to nanoparticle, black box) versus free isotope migrated to the solvent front (green box). (C) Tabulated average values (percentage) obtained from image analysis of TLC in A and B.
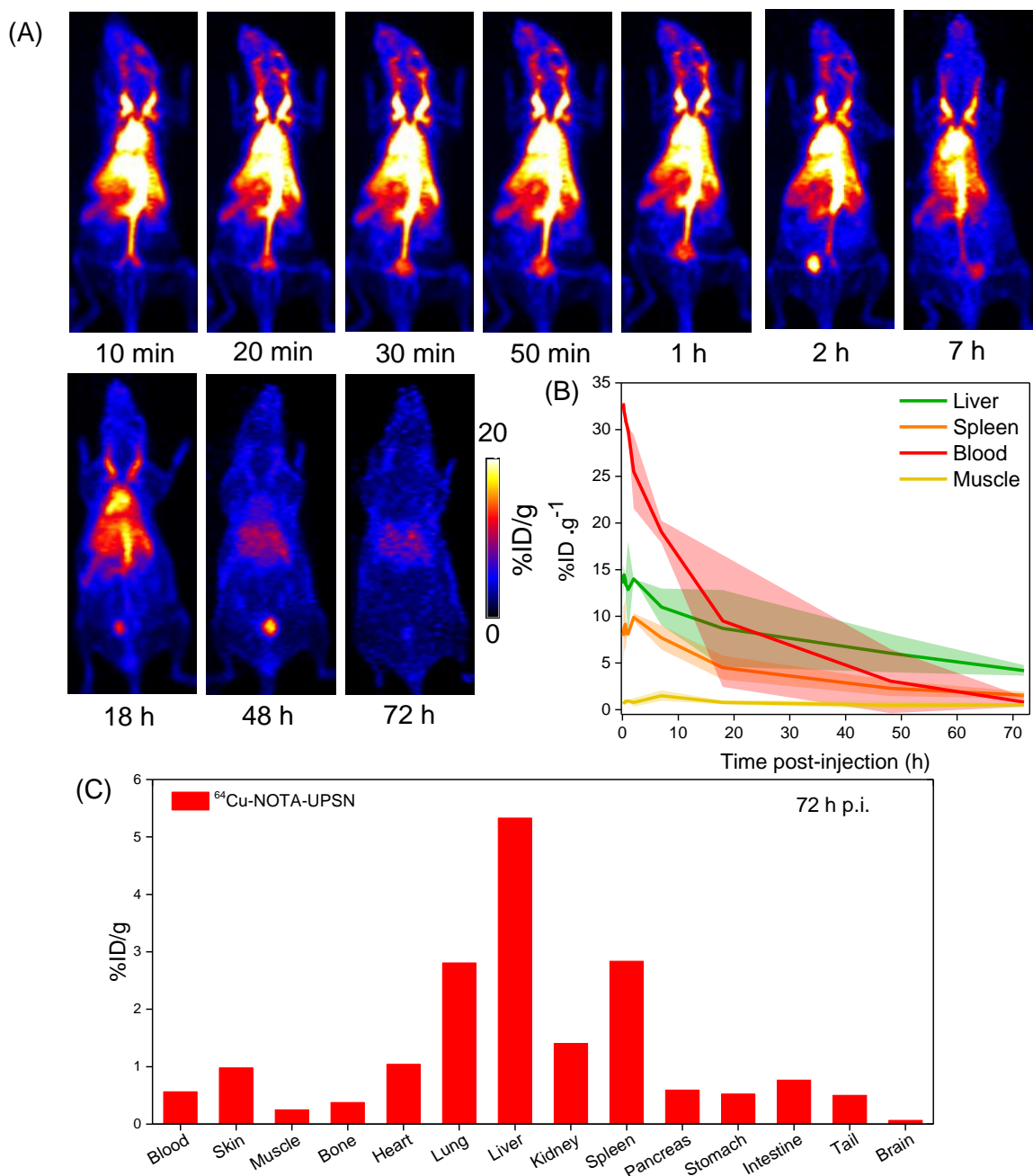
Figure S4. *In vivo* PK of ^{64}Cu-NOTA-UPSN in healthy mice. (A) MIP from dynamic PET scans (upto 1 h p.i., 6 frames of 10 min each) and static scans from 2 h to 72 h p.i. (B) TACs for major organs. (C) *Ex vivo* biodistribution study after terminal PET scan at 48 h p.i. Data represents mean (n= 3).
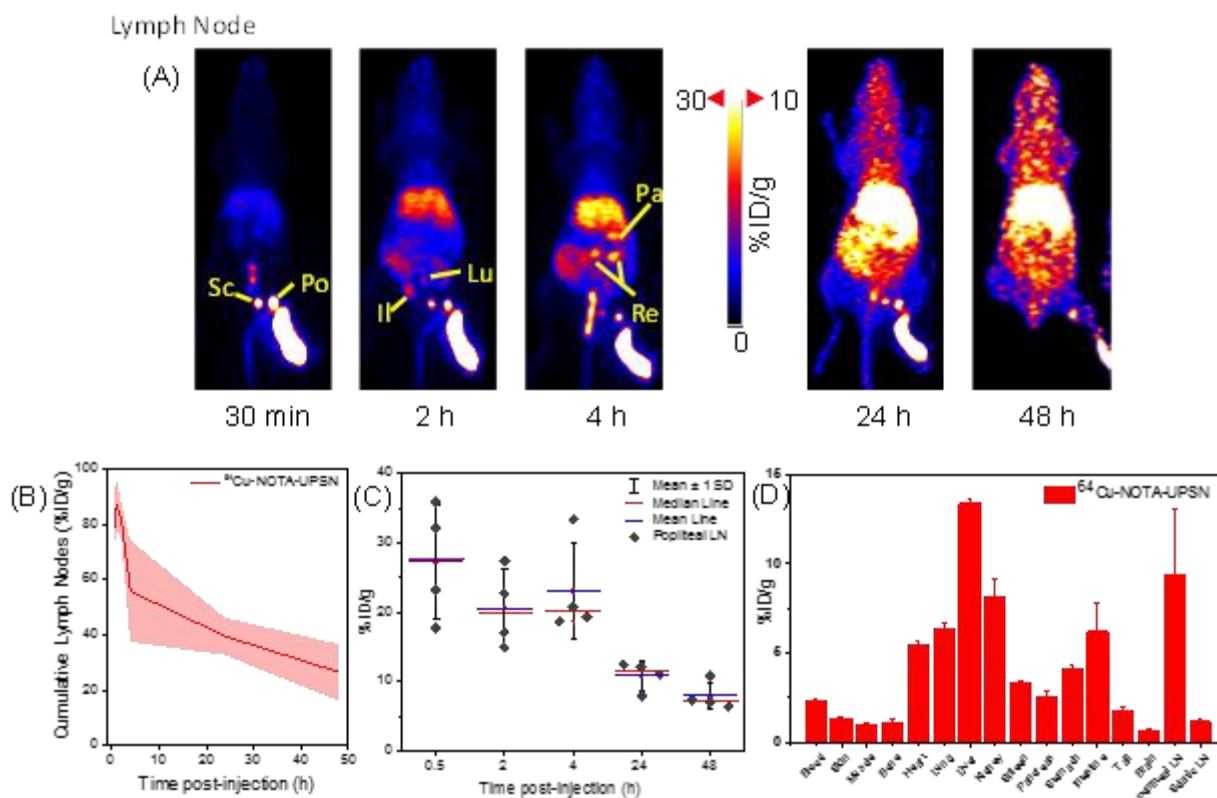
Figure S5. Non-invasive lymph node mapping with ^{64}Cu-NOTA-UPSN. (A) Serial PET MIP depicting progressive lighting up of the lymph nodes 0.5, 2, 4, 24 and 48 h post subcutaneous injection of ^{64}Cu-NOTA-UPSN. (B) Variation in cumulative accumulation of ^{64}Cu-NOTA-UPSN in lymph nodes (mean ± SD, n = 4) over time. (C) Accumulation of ^{64}Cu-NOTA-UPSN in popliteal lymph nodes. Each data point represents one animal. Red line = median, blue line = mean. ((D) Ex vivo gamma counting of major organs and extracted lymph nodes after terminal PET scan at 48 h p.i.
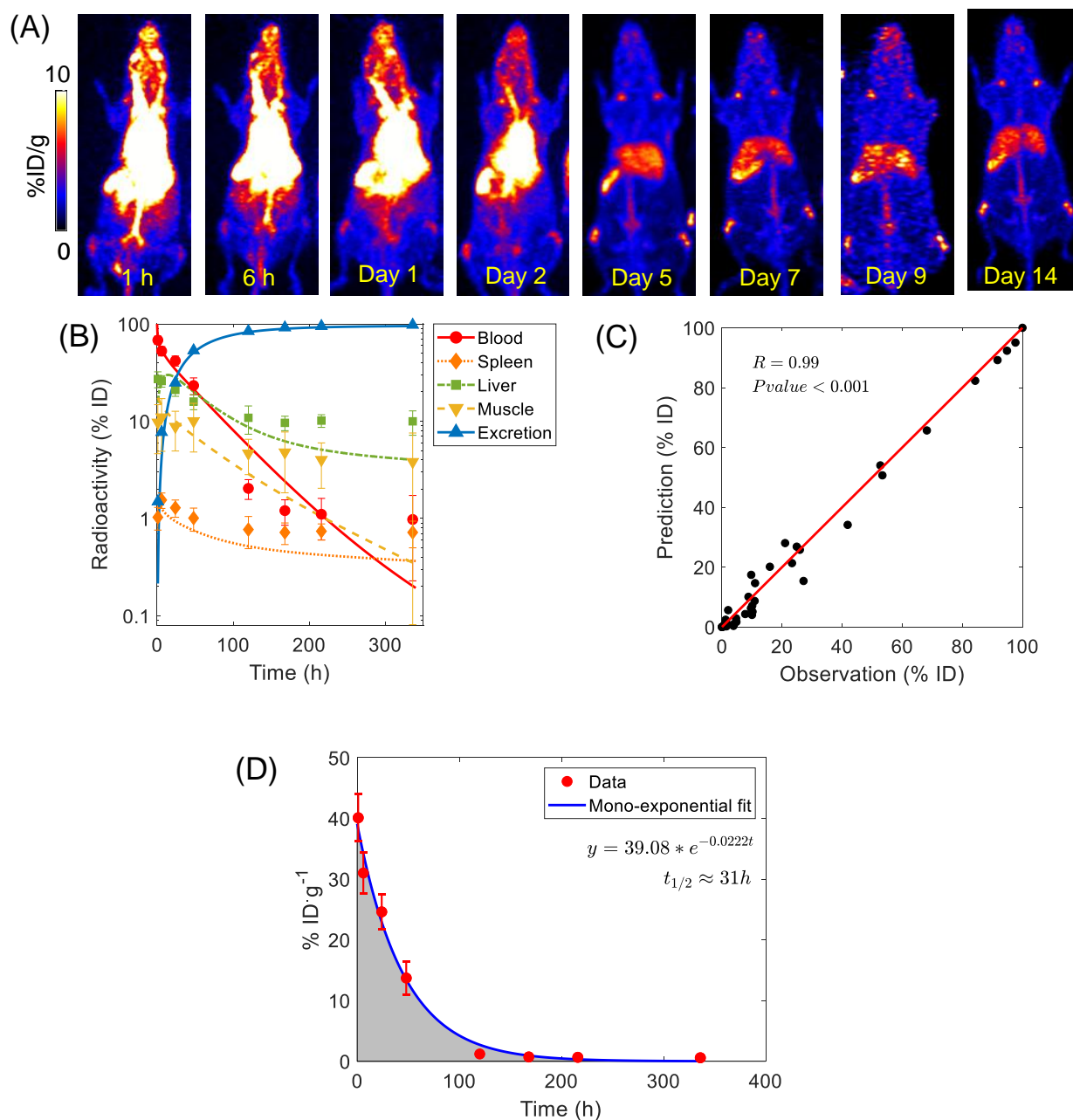
Figure S6. (A) Serial MIP images of healthy mice intravenously injected with ^{89}Zr-DFO-UPSN from metabolic cage studies. (B) Mathematical modelling of NP kinetics. Graph shows the model fits (lines) of the observed values (symbols), plotted on log scale. (C) Pearson correlation analysis indicating a strong positive correlation between the experimental data and model predictions. (E) One-compartment PK model fit of plasma radioactivity concentrations of ^{89}Zr-DFO-UPSN to estimate the elimination half-life ($t_{1/2}$). Data represents mean ± SD (n =4).
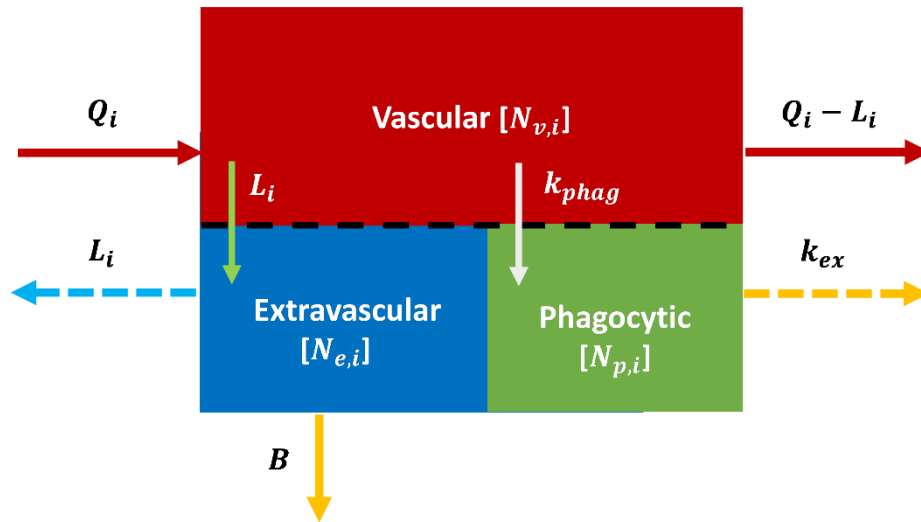
Figure S7. A representative compartment i of the model. The compartment is divided into vascular, extravascular, and phagocytic sub-compartments. The parameters are described in Table S7.
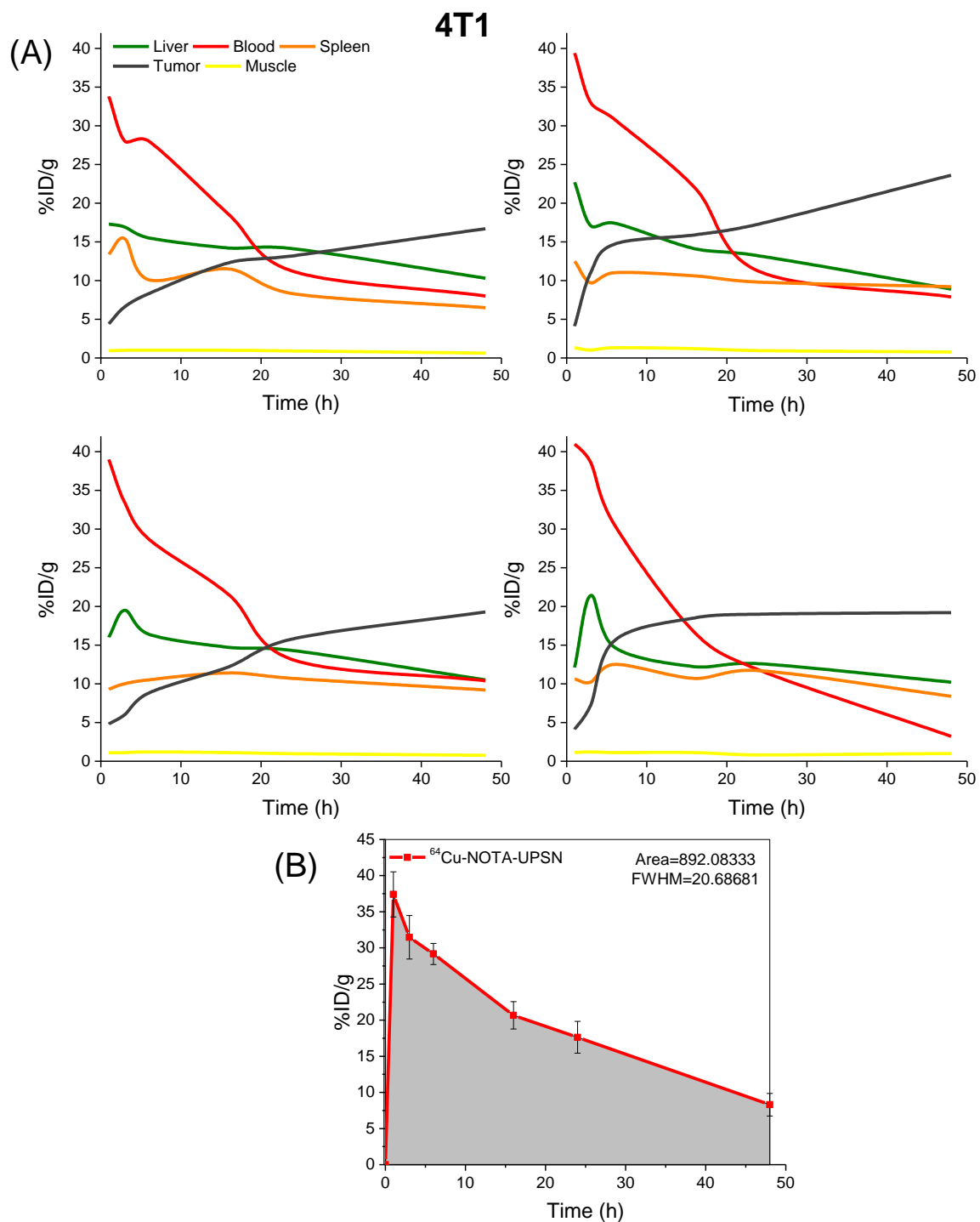
Figure S8. Quantitative ROI analysis of ^{64}Cu-NOTA-UPSN accumulation in 4T1 cohort. (A) TACs of major organs and 4T1 tumor for individual animals. (B) Plasma radioactivity concentration kinetics of ^{64}Cu-NOTA-UPSN in 4T1 tumor-bearing mice.
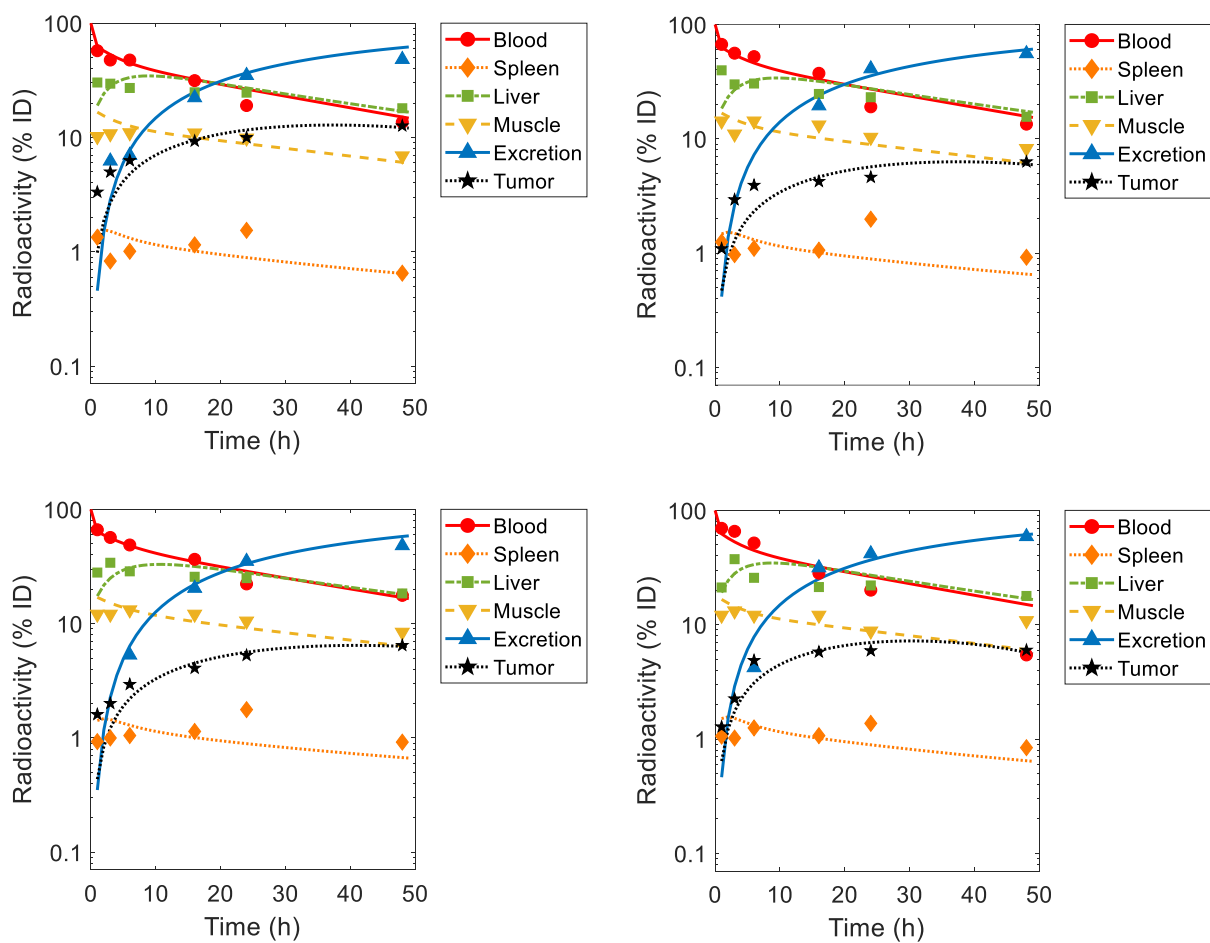
4T1

Figure S9. Mathematical model fits for individual animals in 4T1 cohort.
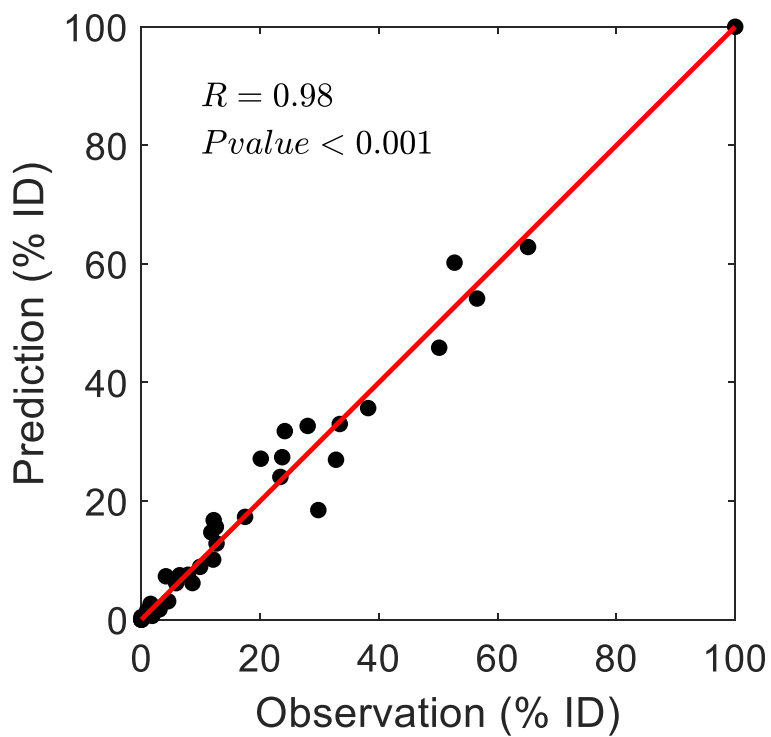
4T1

$R = 0.98$
$Pvalue < 0.001$

Figure S10. Strong positive correlation between observed data and model prediction for the 4T1 group, as indicated by the Pearson Correlation Coefficient (R).
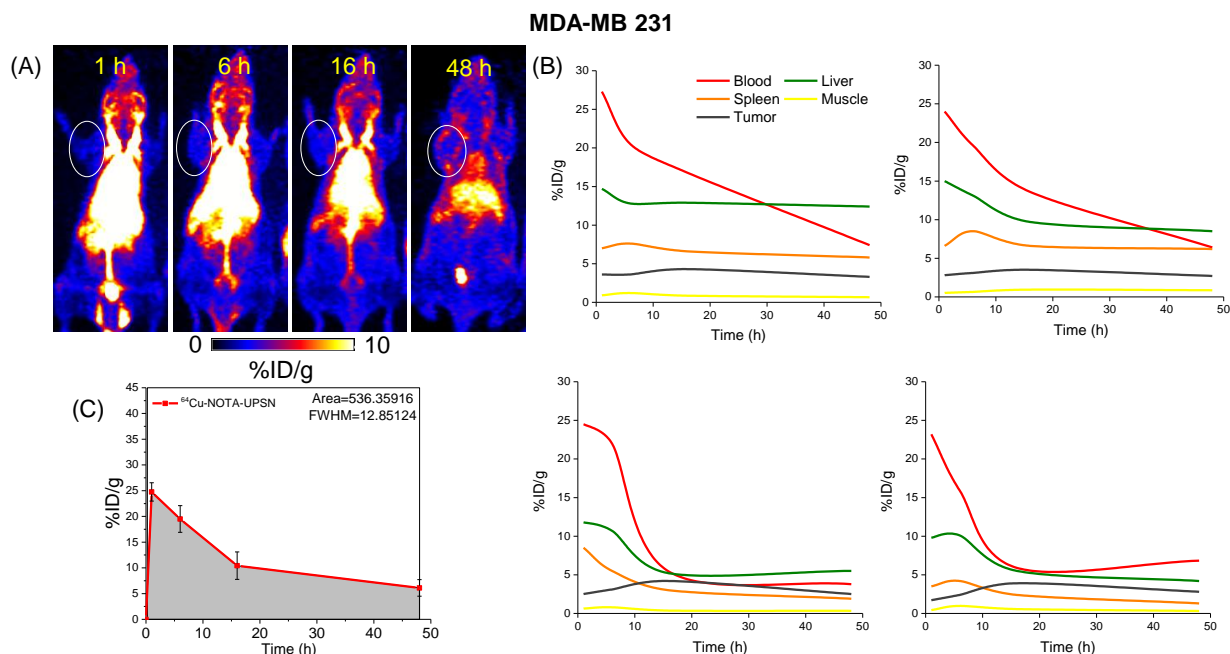

Figure S11. (A) Serial MIP PET images of MDA-MB 231 tumor-bearing mice at a lower scale bar depicting the accumulation of ^{64}Cu-NOTA-UPSN at the tumor margins. (B) TACs of major organs and MDA-MB 231 tumor for individual animals in the cohort. (C) Plasma radioactivity concentration kinetics of ^{64}Cu-NOTA-UPSN in MDA-MB 231 tumor-bearing mice.
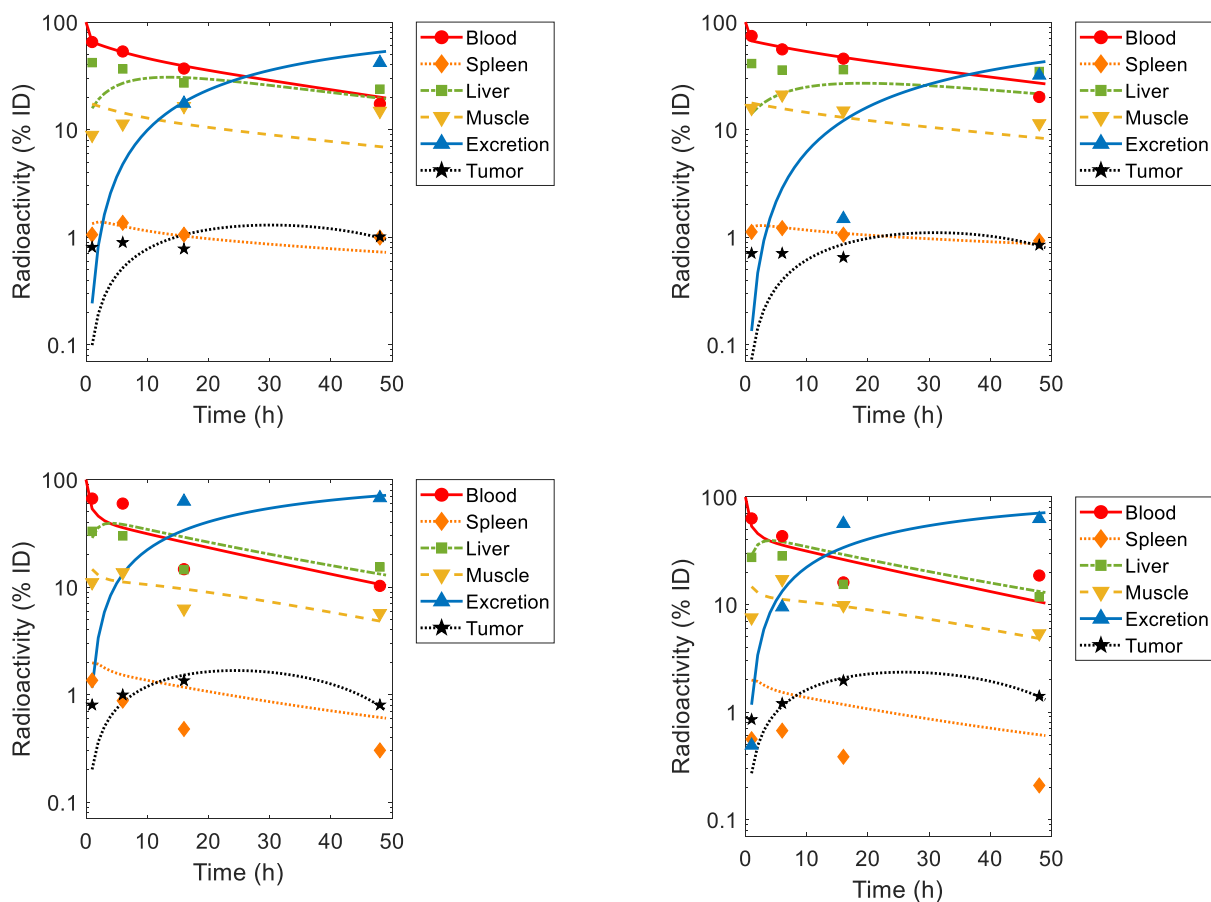
MDA-MB 231

Figure S12. Mathematical model fits for individual animals in MDA-MB 231 cohort.

MDA-MB 231
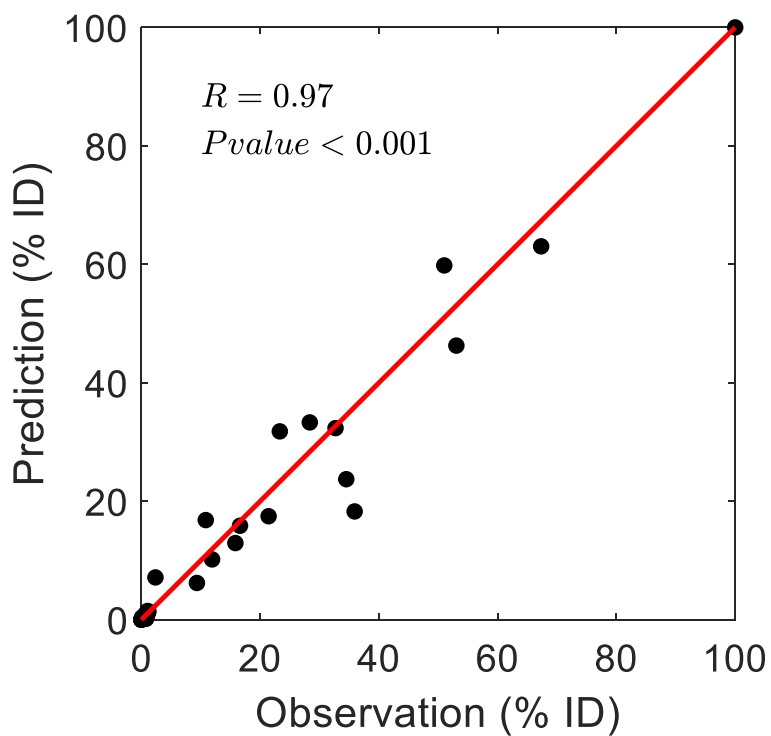

$R = 0.97$
$Pvalue < 0.001$

Figure S13. Strong positive correlation between observed data and model prediction for the MDA-MB 231 cohort, as indicated by the Pearson Correlation Coefficient (R).
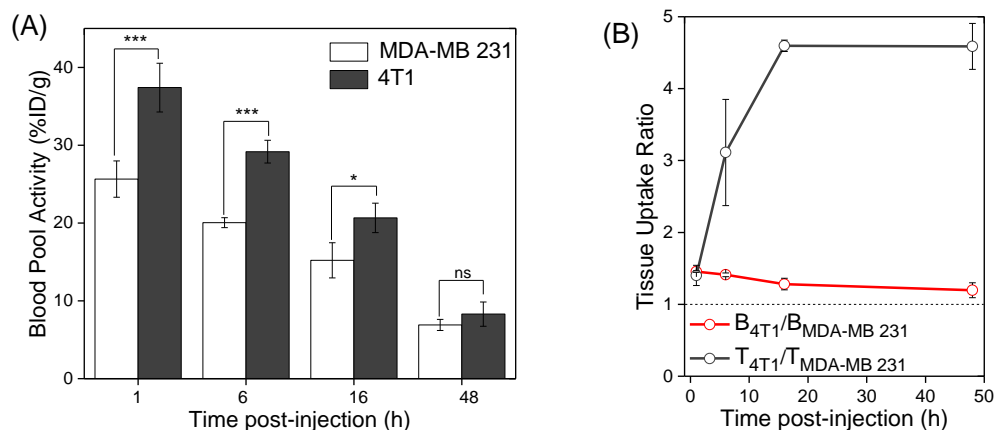

Figure S14. (A) Comparison of blood pool radioactivity between 4T1 and MDA-MB 231 tumor-bearing mice. (B) Decoupling the effect of blood circulation on tumor accumulation of ^{64}Cu-NOTA-UPSN in the two groups.
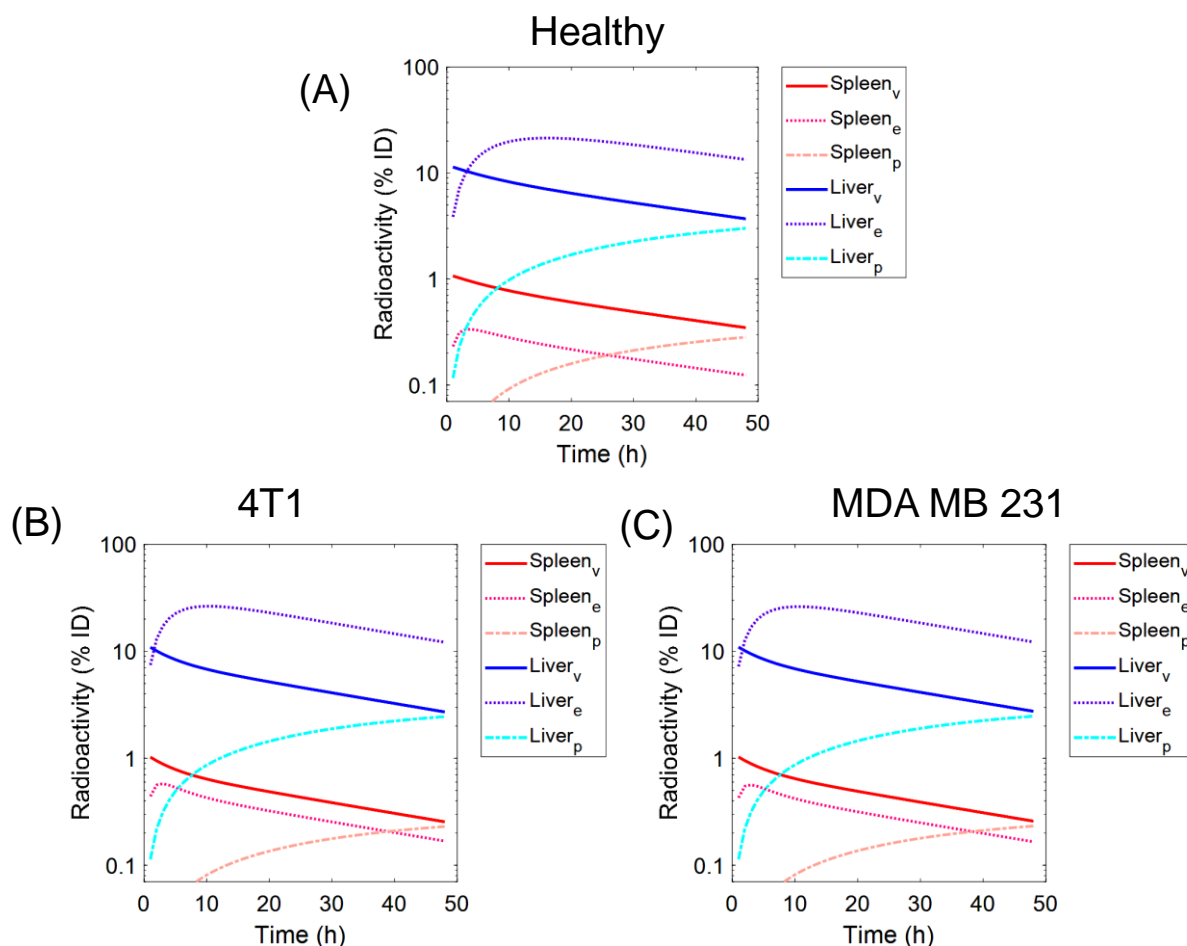

Figure S15. (A) Sub-compartment kinetics of ^{89}Zr-DFO-UPSN in liver and spleen of healthy mice, as predicted by the mathematical model upto 48 h p.i.. (B-C) Sub-compartment kinetics of ^{64}Cu-NOTA-UPSN in liver and spleen in 4T1 and MDA-MB 231 tumor-bearing mice, as predicted by the model.
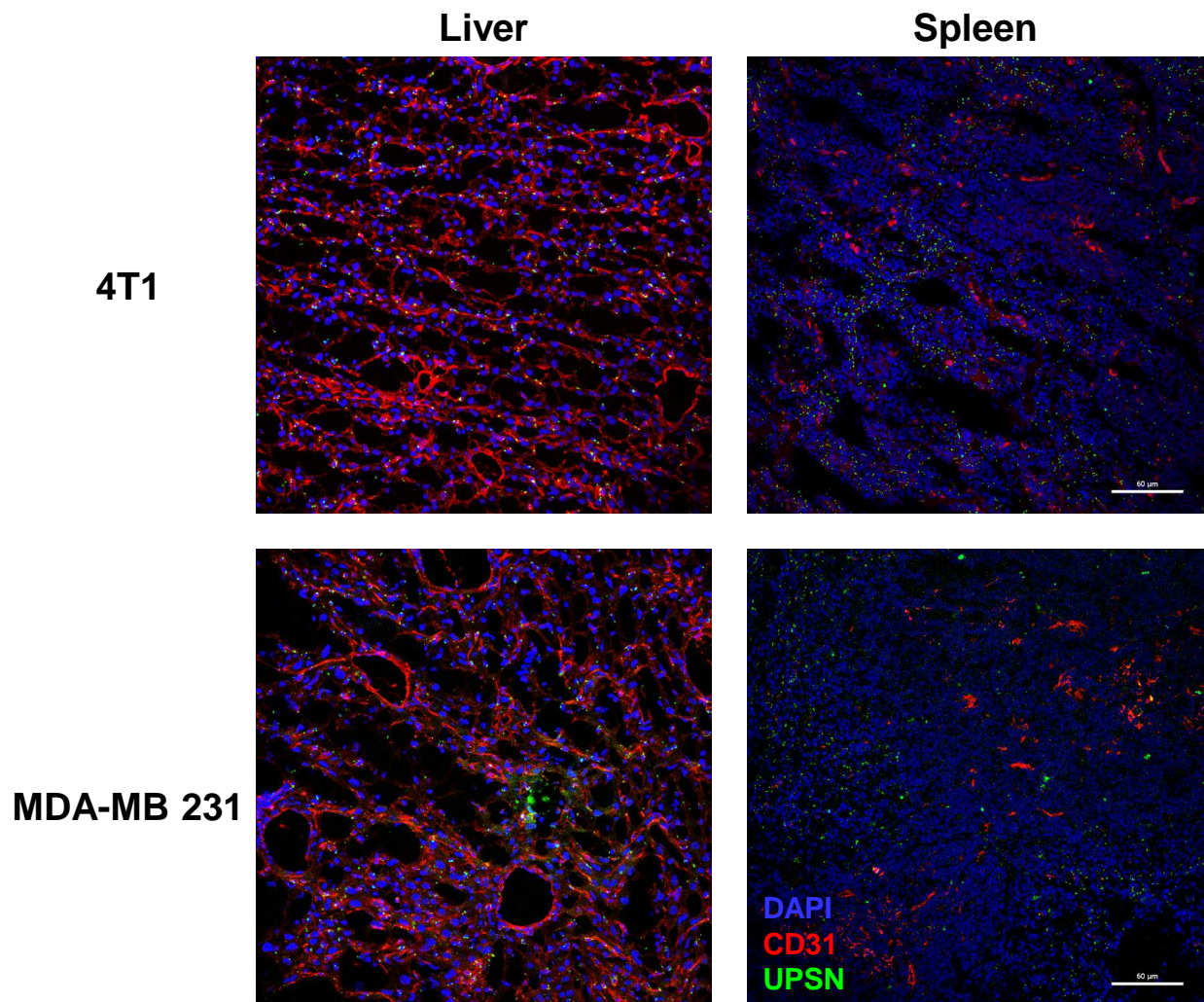
Liver	Spleen

Figure S16. Representative confocal microscopy images of UPSN-FITC (green) and CD31 expressing blood vessels (red) in liver and spleen of 4T1 and MDA-MB 231 tumor-bearing mice. DAPI= nucleus. Scale bar = 50 µm. (n=3)
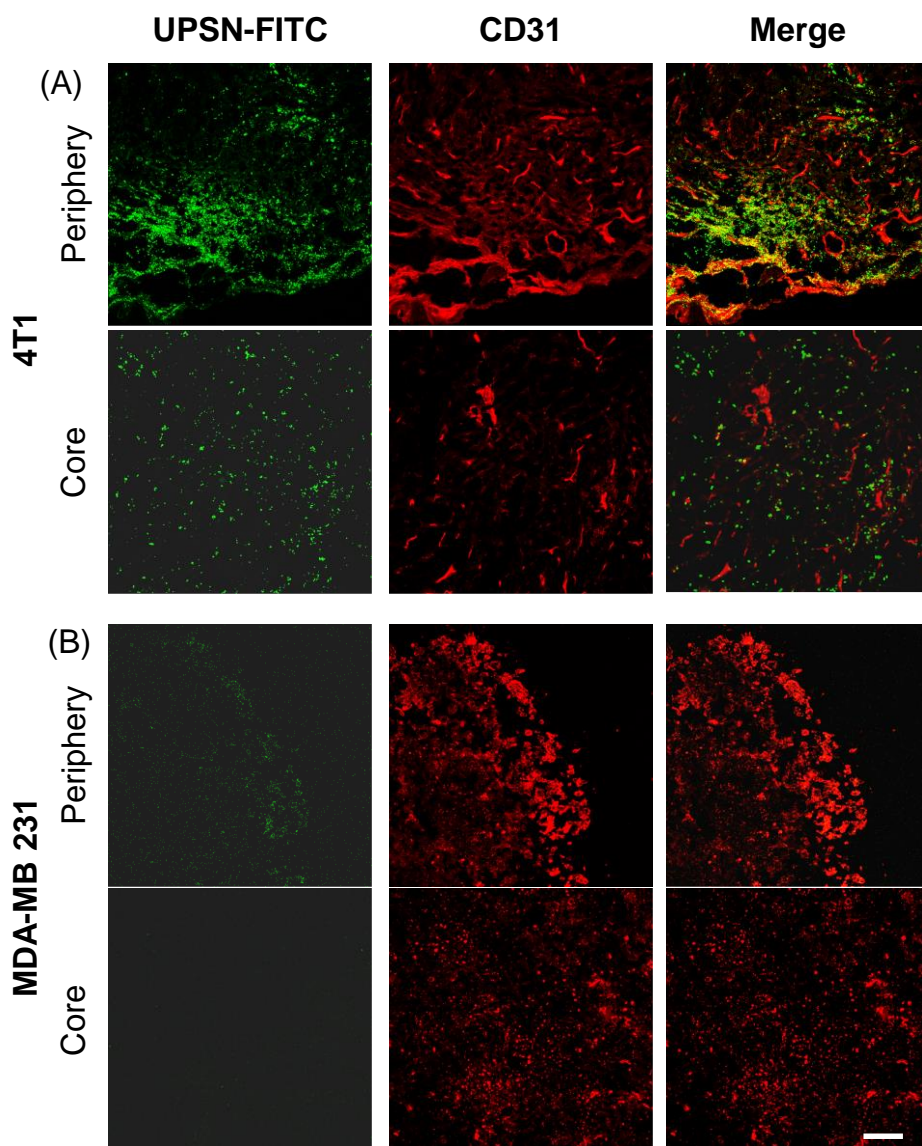
Figure S17. Representative confocal microscopy images showing distribution of UPSN-FITC (green) in relation to CD31 expressing blood vessels (red) in tumor periphery and tumor core in 4T1 and MDA-MB 231 cohorts. Colocalization of UPSNs and blood vessels seen in yellow. Scale bar = 50 µm. (n=3)
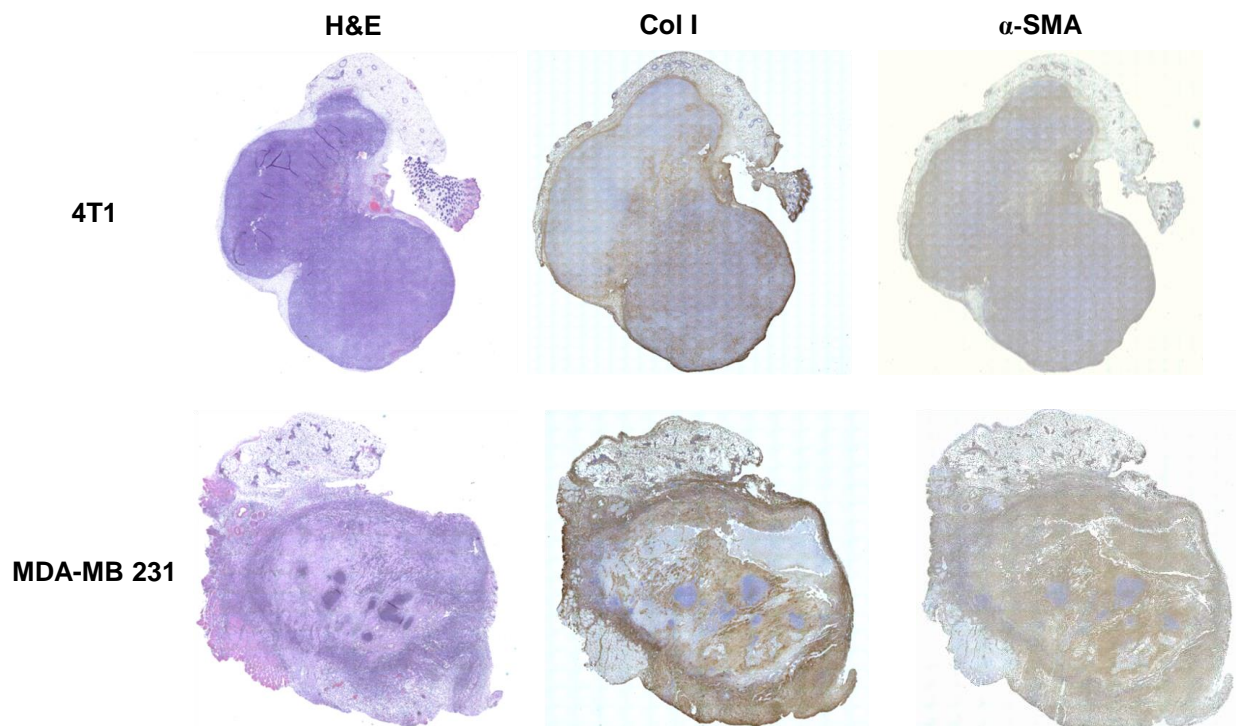
Figure S18. Representative histopathology of whole tissue sections for 4T1 and MDA-MB 231 tumors indicating hematoxylin and eosin (H&E) staining (left), collagen (Col I staining) expression (center), and smooth muscle actin (α-SMA) expression (right). (n = 3)
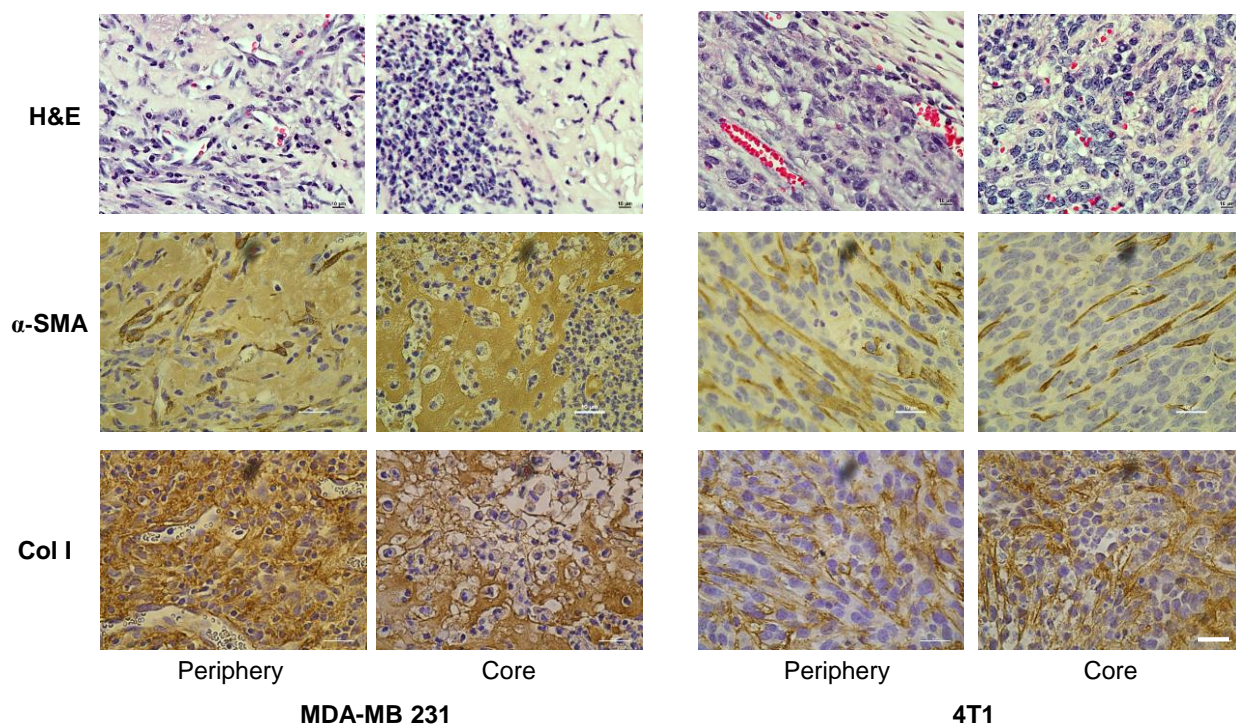
Figure S19. Representative high magnification bright field histological images depicting differences in H&E (top) staining, α-SMA (middle), and col I (bottom) expression in tumor periphery and core, among 4T1 and MDA-MB 231 cohorts (n=3). Scale bar: 10 μm.
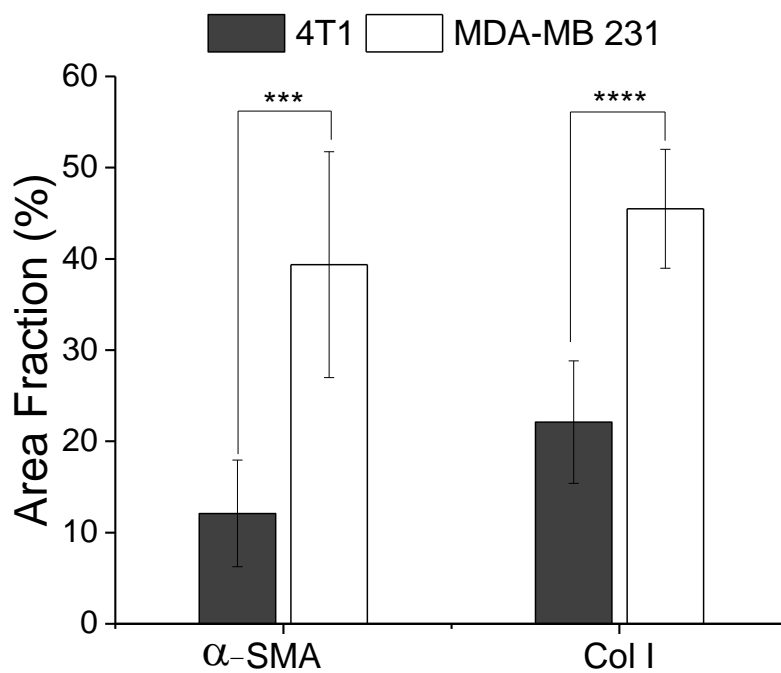
Figure S20. Image analysis of 4T1 and MDA-MB 231 tumors to quantify area fractions (represented as percentage) of α-SMA and col I staining. Data presented as mean ± SD (5 fields of view for n = 3 tumors). *p < 0.05, ** p < 0.01, ***p < 0.001, ****p < 0.0001, ns = non-significant (p > 0.05).

Supplementary Tables

Table S1. Area under the curve (AUC) values in healthy mice injected with [89]Zr-DFO-UPSN and monitored over 14 days. Values indicate exposure (dose per gram of tissue) and cumulative dose deposited in tissues, obtained from experimental observations and model fits.

| Tissue	Exposure (Obs) (%ID•g^{-1}•h)	Cumulative Dose Disposition (Obs) (%ID•h)	Cumulative Dose Disposition (Fit) (%ID•h)
Plasma	1826.2	3188.58352	2962.4
Liver	2362.95	4148.725	3329.8
Spleen	2820.9	282.605	183.8
Muscle	172.33483	1900.54337	1088.2

Table S2. AUC indicating cumulative deposited dose obtained from model predictions in different sub-compartments (v= vascular; e = extravascular; p = phagocytic) of RES organs, liver and spleen, in healthy and tumor-bearing mice.

	Cumulative Dose Disposition (Fit) (%ID•h)					
	Spleen (v)	Spleen (e)	Spleen (p)	Liver (v)	Liver (e)	Liver (p)
Healthy (0-340 h)	47.4	16.7	119.5	505.3	1551.9	1272.5
Healthy (0-48 h)	28.4	9.9	8.1	302.9	822.1	86.4
4T1 (0-48 h)	23.1	15.1	6.8	246.6	923.1	72.5
MDA MB 231 (0-48 h)	23.3	14.8	6.8	248.9	920.3	73.1

Table S3. Least squares estimates of UPSN inflow rate (k_{in}), and outflow rate (k_{out}) for individual 4T1 tumor-bearing mice, as obtained from the PBPK model fitting.

4T1	k_{in} (h^{-1})	k_{out} (h^{-1})
Mouse 1	0.015	0.0056
Mouse 2	0.0071	0.0028
Mouse 3	0.0066	0.0025
Mouse 4	0.0098	0.005

Table S4. Least squares estimates of UPSN inflow rate (k_{in}), and outflow rate (k_{out}) for individual MDA-MB 231 tumor-bearing mice, as obtained from the PBPK model fitting.

MDA-MB 231	k_{in} (h^{-1})	k_{out} (h^{-1})
Mouse 1	0.0015	0.0012
Mouse 2	0.0011	0.0014
Mouse 3	0.0034	0.0015
Mouse 4	0.0045	0.0018

Table S5. Comparison of UPSN inflow (k_{in}) and outflow (k_{out}) rates for the two tumor models. Data represents mean ± SD, n = 4.

Tumor	k_{in} (h^{-1})	k_{out} (h^{-1})
4T1	0.0096 ± 0.0038	0.004 ± 0.0015
MDA-MB 231	0.0026 ± 0.0016	0.0015 ± 0.0002

Table S6. AUC indicating cumulative dose deposition (observed or model fit) in major organs and tumors obtained by PBPK modeling for the two tumor models. Data represents mean ± SD, n = 4.

Tissue	Cumulative Dose Disposition (Obs) (%ID•h)		Cumulative Dose Disposition (Fit) (%ID•h)	
	4T1	**MDA-MB 231**	**4T1**	**MDA-MB 231**
Plasma	1386.4 ± 99.5	1509 ± 392.5	1473.5 ± 54.1	1518 ± 458
Liver	1114.8 ±47.9	1185.1 ±423.8	1241.5 ± 0.65	1178.9 ± 31.6
Spleen	57.8 ± 5.0	36.2 ± 16.8	45.1 ± 0.05	48.9 ± 2.01
Tumor	289.7 ±110.6	50.6 ± 17.7	303.3 ± 116.3	59.2 ± 20.6

Table S7. PBPK model parameter values as obtained from the literature, or estimated through non-linear regression.

Parameter	Definition	Value	Reference
Q_l	Plasma flow rate into liver via hepatic artery	10.3 ml·h^{-1}	[3]
Q_g	Plasma flow rate from gut into liver via portal vein	75.4 ml·h^{-1}	[3]
Q_s	Plasma flow rate into spleen	8.18 ml·h^{-1}	[3]
Q_m	Plasma flow rate into muscle	86.1 ml·h^{-1}	[3]
$V_{v,l}$	Volume of vascular space in liver	0.298 ml	[3]
$V_{v,s}$	Volume of vascular space in spleen	0.028 ml	[3]

$V_{v,m}$	Volume of vascular space in muscle	0.453 ml	[3]
$V_{e,l}$	Volume of extravascular space in liver	1.6246 ml	[3]
$V_{e,s}$	Volume of extravascular space in spleen	0.099 ml	[3]
$V_{e,m}$	Volume of extravascular space in muscle	10.8666 ml	[3]
V_p	Volume of blood	1.717 ml	[3]
B	Bile flow rate	0.0833 ml·h^{-1}	[4]
σ_l	Reflection coefficient of microvasculature in liver	0	Arbitrary
σ_s	Reflection coefficient of microvasculature in spleen	0	Arbitrary
σ_m	Reflection coefficient of microvasculature in muscle	0.98	Estimated from non-linear regression in Fig. 2D
k_{phag}	Phagocytic uptake rate constant	0.01 h^{-1}	Estimated from non-linear regression in Fig. 2D
k_{ex}	Phagocytic excretion rate constant	0.001 h^{-1}	[5]
k_{in}	NP inflow rate constant into tumors	Tables S3, S4, S5	Estimated from non-linear regression in Fig. 3D, 3E
k_{out}	NP outflow rate constant from tumors	Tables S3, S4, S5	Estimated from non-linear regression in Fig. 3D, 3E
L_i	Lymph flow rates in organ i (liver, spleen, muscle)	$1/f$ times the corresponding plasma flow rates	Estimated through non-linear regression in Figs 2D, 3D, 3E

References

1. Yuan, D.; He, H.; Wu, Y.; Fan, J.; Cao, Y., *J Pharm Sci* **2018**.
2. Choi, H. S.; Liu, W.; Misra, P.; Tanaka, E.; Zimmer, J. P.; Ipe, B. I.; Bawendi, M. G.; Frangioni, J. V., *Nat Biotechnol* **2007,** *25* (10), 1165.
3. Shah, D. K.; Betts, A. M., *J Pharmacokinet Pharmacodyn* **2012,** *39* (1), 67-86.
4. Gabrielsson, J.; Weiner, D., *Pharmacokinetic and pharmacodynamic data analysis: concepts and applications*. CRC Press: **2001**; Vol. 2.
5. Lin, Z.; Monteiro-Riviere, N. A.; Riviere, J. E., *Nanotoxicology* **2016,** *10* (2), 162-72.